Research Repository UCD

Title	Conversion of amorphous TiO2 coatings into their crystalline form using a novel microwave plasma treatment
Authors(s)	Dang, Binh H.Q., Rahman, Mahfujur, MacElroy, J. M. Don, Dowling, Denis P.
Publication date	2011-07-25
Publication information	Dang, Binh H.Q., Mahfujur Rahman, J. M. Don MacElroy, and Denis P. Dowling. “Conversion of Amorphous TiO2 Coatings into Their Crystalline Form Using a Novel Microwave Plasma Treatment.” Elsevier, July 25, 2011. https://doi.org/10.1016/j.surfcoat.2011.03.075.
Publisher	Elsevier
Item record/more information	http://hdl.handle.net/10197/2896
Publisher's version (DOI)	10.1016/j.surfcoat.2011.03.075

Downloaded 2026-05-02 00:29:03

The UCD community has made this article openly available. Please share how this access benefits you. Your story matters! (@ucd_oa)

© Some rights reserved. For more information

Conversion of amorphous TiO_2 coatings into their crystalline form using a novel microwave plasma treatment

Binh H. Q. Dang [1], Mahfujur Rahman [1], Don MacElroy [1], and Denis P. Dowling [1,2,*]

[1] School of Chemical & Bioprocess Engineering, University College Dublin, Ireland

[2] School of Mechanical & Materials Engineering, University College Dublin, Ireland

* Corresponding author,

Dr. Denis P. Dowling

Room 223, UCD Engineering & Materials Science Center,

University College Dublin, Belfield, Dublin 4, Republic of Ireland

Tel: (+353) 1 716 1747

Fax: (+353) 1 283 0534

E-mail: denis.dowling@ucd.ie

Abstract

Crystalline titanium dioxide (TiO_2) coatings have been widely used in photo-electrochemical solar cell applications. In this study, TiO_2 and carbon-doped TiO_2 coatings were deposited onto unheated titanium and silicon wafer substrates using a DC closed-field magnetron

sputtering system. The resultant coatings had an amorphous structure and a post-deposition heat treatment is required to convert this amorphous structure into the photoactive crystalline phase(s) of TiO_2. This study investigates the use of a microwave plasma heat treatment as a means of achieving this crystalline conversion. The treatment involved placing the sputtered coatings into a 2.45 GHz microwave-induced nitrogen plasma where they were heated to approximately 550°C. It was observed that for treatment times as short as 1 minute, the 0.25-μm thick coatings were converted into the anatase crystalline phase of TiO_2. The coatings were further transformed into the rutile crystalline phase after treatments at higher temperatures. The doping of TiO_2 with carbon was found to result in a reduction in this phase transformation temperature, with higher level of doping (up to 5.8% in this study) leading to lower anatase-to-rutile transition temperature. The photoactivity performance of both doped and un-doped coatings heat-treated using both furnace and microwave plasma was compared. The carbon-doped TiO_2 exhibited a 29% increase in photocurrent density compared to that observed for the un-doped coating. Comparing carbon-doped coatings heat-treated using the furnace and microwave plasma, it was observed that the latter yielded a 19% increase in photocurrent density. This enhanced performance may be correlated to the differences in the coatings' surface morphology and band gap energy, both of which influence the coatings' photoabsorption efficiency.

Keywords: titanium dioxide, magnetron sputtering, carbon doping, microwave plasma, phase transformation

1. Introduction

Titanium dioxide thin films have been studied intensively in recent years due to their applicability in areas as diverse as electrochromics, photocatalysis, and photovoltaic solar cells [1-4]. Among the many thin film deposition techniques used, magnetron sputtering in general and DC closed-field magnetron sputtering in particular have been shown to yield coatings exhibiting very good substrate adhesion [5]. This is particularly important for the use of TiO_2 coatings in water-splitting processes for example where the coated electrode is immersed into water. The structure of the sputtered TiO_2 thin films, however, has been shown to be strongly dependent on the sputter deposition conditions [6-8]. In the absence of high substrate temperatures, amorphous TiO_2 coatings are generally obtained. Subsequent heat treatments are therefore required to convert the titania coatings into their photoactive crystalline phases, namely anatase, rutile, and brookite [9]. Of these three TiO_2 polymorphs, the thermodynamically stable rutile and the metastable anatase are the more common forms of titania, with anatase starting to convert irreversibly into rutile upon heat treatment at temperatures between 400°C and 1200°C [9-11]. Anatase has been reported to be photoactive under UV illumination only, while rutile exhibits activity in both the UV and a small part of the visible spectrum range due to its lower band gap. Its level of photoactivity is however lower than that of anatase due to the high recombination rate of its photo-generated electrons and holes [12]. Coatings of mixed-phase TiO_2 have been found to have better performance than those of pure phases alone, with the relative composition of anatase to rutile being a key parameter dictating the coatings' photoactivity and hence applications [13-15]. Chou et al. reported that, upon a 2-hour air furnace heat treatment of a co-sputtered C-doped TiO_2, the amorphous coating transformed partially into rutile (10% by mass) at 800°C [16]. When the same treatment was carried out under vacuum however, the amorphous coating

transformed completely into rutile at 300°C. These investigators proposed that both carbon incorporated in titania and an oxygen-deficient environment facilitated the phase transformation into rutile. In this study, a more systematic investigation on how the carbon dopant concentration influenced both the level and temperature of the anatase-to-rutile phase transformation was carried out. The need for an oxygen-deficient environment to favor the rutile formation was also re-examined.

Furnace heat treatment is usually employed to obtain the TiO_2 phase transformation but the overall processing time generally takes more than an hour due to the ramping-up and cooling-down times. Microwave (without the use of plasma) has also been investigated as an alternative more rapid heat treatment method. It was reported that, for un-doped TiO_2 powder, the anatase-to-rutile phase transition occurred after a 30-minute treatment at a temperature of approximately 800°C [17]. In this study, the use of a microwave (MW) plasma was investigated for the first time as an alternative heat treatment method to achieve this amorphous TiO_2 to crystalline phase(s) conversion. The photoactivity performance of the heat-treated coatings was also assessed using photocurrent density measurements as these have been shown to indicate the potential of the coatings for use in water-splitting processes [8,18].

2. Experimental procedures

2.1. Deposition of TiO_2 and its C-doped coatings – TiO_2 thin films were deposited using a Teer Coatings UDP-450 DC closed-field magnetron sputtering system onto titanium and p-type Si(100) substrates supplied by Compart Technology Ltd. These substrates had first been ultrasonically cleaned in methanol followed by acetone prior to coating deposition. Pure titanium (99.5%) of size 300 mm x 100 mm x 2 mm was used as the sputtering target and distanced 100

mm away from the 2-rpm rotatable substrate holder. High-graded argon (99.998%) was used as the sputtering gas while oxygen (99.9%) and carbon dioxide (99.8%) were used as the reactive gases where needed. Before deposition, the target and the substrates were sputtered cleaned in an argon plasma for 20 minutes (working pressure of $2x10^{-3}$ mbar, target current of 0.2A, and substrate bias voltage of -400V). The sputtering condition was then changed to $4x10^{-3}$ mbar of working pressure, 2A of target current, and -50V of substrate bias voltage before oxygen was passed in. The oxygen flow rate was set by a reactive sputtering controller, monitoring the Ti peak, so as to form stoichiometric TiO_2 [8]. C-doped TiO_2 coatings were obtained by further introducing carbon dioxide of different flow rates (1 – 5 sccm) into the chamber. Sputtering time was varied from 30 to 60 minutes in order to obtain coatings with similar thickness.

2.2. Thermal treatments – The coatings were treated in both a box furnace and a MW plasma chamber. In the case of the latter, a circumferential antenna plasma (CAP) microwave system was used [19]. The chamber was first pumped down to 0.1 mbar at which point 50 sccm of nitrogen gas (99.998%) was introduced and the pressure was adjusted to 5 mbar using a manual throttle valve. The microwave discharge was then ignited to form a plasma ball around the samples located in the center of the chamber. Input powers of 2.4 kW were provided from a Mugge microwave power supply operating at 2.45 GHz. Sample temperatures were measured using a LASCON QP003 two-color pyrometer from Dr. Mergenthaler GmbH & Co. The coated samples were treated at temperatures of approximately 550, 750, 800, 850, and 875°C for periods between 1 and 10 minutes. A Carbolite CWF 1200 chamber furnace was used for air heat-treating the coatings. The chamber was first heated up to 750°C (ramping 20°C/min) at which point the samples were placed in for 3 minutes and then removed.

2.3. Characterization techniques – The degree of crystallinity and the phase composition of the films on silicon substrate were examined by a Siemens D500 X-ray diffractometer (XRD) operating at 40kV and 30mA with Cu Kα radiation at a wavelength of 0.1542 nm. The scan was in 2θ mode and spanned from 20° to 80° with steps of 0.02° per second. X-ray photoelectron spectroscopy (XPS) analysis of the samples was carried out using a Kratos AXIS 165 spectrometer with a monochromatic Al Kα radiation (hv = 1486.58eV). The surface morphology of the films was visualized using an FEI Quanta 3D FEG DualBeam system. Surface roughness was measured using a WYKO NT1100 optical profilometer in vertical scanning interferometry (VSI) mode. Film thicknesses and optical constants were measured using a Woollam M-2000 variable wavelength ellipsometer. The ellipsometric data were recorded at incident angles of 65°, 70°, 75° and the measurements were fitted to a four-phase model which consists of a Si substrate, a SiO_2 interfacial layer (fixed at 2 nm), a fittable Tauc-Lorentz TiO_2 thin film layer, and a surface roughness layer whose value had been obtained from optical profilometer [20] . Photocurrent (I_{ph}) measurements were carried out with the films on titanium substrate using a custom-made photo-electrochemical (PEC) cell, a Gamry G300 potentiostat, and a Newport 450W (xenon arc lamp) solar simulator [8]. The PEC cell consisted of three electrodes – the working electrode, the counter electrode, and the reference electrode – all immersed in an aqueous electrolyte solution of 1M NaOH.

3. Results and Discussion

The initial study focused on the characterization of the sputter deposited coatings. The objective in particular was to determine how the level of CO_2 addition into the sputtering chamber during TiO_2 coating deposition influenced the coating properties.

3.1. XPS – Fig. 1a demonstrates how the variation in CO_2 flow rates from 1 to 5 sccm during sputtering influenced the elemental data obtained for the C-doped coatings. The titanium concentration remains relatively constant for all five coatings whereas the oxygen concentration decreases with increasing flow rate of CO_2 up to 3 sccm and increases thereafter. The carbon concentration, however, follows the opposite trend to the oxygen concentration. A possible explanation for the decrease in carbon concentration at CO_2 flow rates above 3 sccm may be due to quenching of the plasma or alternatively some poisoning of the titanium target. The overall effect is the reduction in doped TiO_2 coating growth rate from 5.1 nm/min at CO_2 flow rate of 3 sccm to 4.1 nm/min for deposition at 5 sccm of CO_2.

The XPS spectra of C1s state for the 2.2% C-doped coatings (deposited at 4 sccm of CO_2) is given in Fig. 1b. The as-deposited sample exhibits peaks for simple carbon (C–C, 284.8eV) and carbide carbon (Ti–C, 282.4eV) [13], with the latter being evidence for the presence of carbon dopants (2.2%) in the coating. A comparison is made between the XPS spectra for the TiO_2 coatings thermally treated in the furnace and MW plasma for 3 minutes at 750°C. As illustrated in Fig. 1b, there are relatively small variations in the C–C peak intensity while the Ti–C peak intensity decreases significantly for the MW plasma-treated sample and completely disappears for the furnace-treated coating. This reduction in Ti–C peak intensity is associated with the loss of carbide carbon and may be associated with its reaction with oxygen in titania forming volatile carbon oxide species and thus generating oxygen vacancies. The higher carbide carbon loss after furnace treatment may be due to its further reaction with oxygen in the air. The loss of Ti–C carbon in the coating treated in the air environment indicates that it is not necessary for vacuum to be present in order to facilitate the formation of oxygen vacancies. This conclusion is different in some extent from that observed by Chou et al. who proposed that oxygen vacancies

could only be created favorably when the coatings were treated in an oxygen-deficient environment [16].

3.2. XRD – Fig. 2a shows the evolution of coating crystallinity with MW plasma treatment for the un-doped TiO_2 films. After treatment at 550°C, peaks due to the anatase phase were observed in the diffraction spectra. This single phase was observed at all temperatures up to 875°C at which point peaks for rutile were also observed. Using the equation $f_R = 1 / [1 + (0.884 I_A/I_R)]$ by Spurr and Myers [21] where I_A and I_R represent the integral intensities of the anatase peak A(101) and the rutile peak R(110) respectively, the mass fraction of rutile (f_R) in the coating treated to 875°C was determined to be 17%. When the same study was repeated for 2.2% C-doped TiO_2, the corresponding rutile concentration was found to be 100% (Fig. 2b). For the doped oxide also, the rutile phase began to emerge after treatment at 750°C. The rutile concentrations observed after treatments at 750, 800, and 850°C were 34, 35, and 43% respectively. From this MW plasma treatment study, it was confirmed that C-doping lowered the anatase-to-rutile transition temperature.

To further investigate the effect of carbon dopant concentration on phase composition, XRD analysis was also performed on the C-doped TiO_2 coatings deposited at different flow rates of CO_2. These coatings were each MW plasma-treated at 750, 800, and 850°C for 3 minutes (Fig. 3). From this figure, it is clear that the pattern of rutile mass fraction closely correlates with the pattern of carbon uptake shown in Fig. 1a. This correlation suggests that the higher the carbon dopant concentration, the more favorable is the anatase-to-rutile transformation. Crystallographically, anatase can be considered as an arrangement of $[TiO_6]$ octahedrons where each octahedron is in contact with eight neighbors, four sharing edge oxygen pairs and four sharing corner oxygen atoms [22]. In the rutile structure, each octahedron is in contact with ten

neighbors, two sharing an edge and eight sharing a corner [22]. An oxygen vacancy may destroy two edge-sharing octahedrons and favor the formation of two corner-sharing units in a manner similar to that described in [16]. Since rutile has a higher ratio of corner-sharing octahedrons, an oxygen vacancy may thus favor the formation of rutile over anatase. XPS results suggested that C-doping generates such oxygen vacancies during heat treatment and may therefore explain the favorable effect of C-doping on rutile formation as demonstrated by the XRD results.

XRD analysis was also used to compare the phase transformation efficiency of the furnace and MW plasma treatments of the TiO_2 coatings. Table 1a compares the degree of crystallinity of un-doped and 2.2% C-doped TiO_2 coatings treated by both methods for 3 minutes at 750°C. The results demonstrate that comparable crystal contents were obtained after both treatments. It is interesting however to compare the processing efficiency of the two heat treatment techniques. The resistance furnace treatment took approximately 75 minutes in total (72 minutes of heating up and cooling down plus 3 minutes of treatment) whereas localized volumetric heating by MW plasma only took 13 minutes (5 minutes of setting up, 3 minutes of up-ramping and treatment, and 5 minutes of chamber cooling) – approximately 83% more time-efficient. Due to the differences in heating mechanism, there are also some variations in the surface morphology of the coatings treated by furnace and MW plasma. Fig. 4 shows SEM images of samples deposited on titanium substrate and it is clear that after the MW plasma treatment, the coating exhibited a rougher surface than that obtained after the furnace treatment. This observation was supported using optical profilometry measurements of coatings deposited on silicon wafer substrate (Table 1b). Both the average roughness (R_a) and root mean square roughness (R_q) are higher for the MW plasmas-treated versus the furnace-treated coatings.

3.3. Band gap measurements – The extinction coefficient k for the coatings was obtained from the ellipsometry measurements. The absorption coefficient α was then calculated via the relationship $\alpha = 4\pi k/\lambda$ where λ is the wavelength of the incident light. The indirect band gap E_g was determined using the relation $(\alpha hv)^{1/2} = B \cdot (hv - E_g)$ [23] where B is a constant and hv is the incident photon energy. The variations of $(\alpha hv)^{1/2}$ versus hv for the ~250 nm thick coatings are shown in Fig. 5a. E_g values were determined from the x-intercepts of the linear portion of the graphs in correspondence of $\alpha = 0$. The band gaps were estimated to be 3.37eV for MW plasma-treated un-doped coating and 3.39eV, 3.23eV, and 3.15eV for as-deposited, furnace-treated, and MW plasma-treated 2.2% C-doped coatings respectively. Broadly similar values were also obtained from direct Tauc-Lorentz parameterization using the CompleteEASE software by J.A. Woollam. These values were found to agree with those reported by Tanemura et al. [24].

3.4. Photocurrent density measurements – Fig. 5b plots the photocurrent density measurements for the coatings whose band gaps had been measured earlier. At ~0.23V vs. SCE (1.23V vs. RHE) which is the minimum theoretical voltage required to split water in a PEC cell, there is a 19% increase in photocurrent density produced by the MW plasma-treated C-doped coating (216 $\mu A/cm^2$) compared to the furnace-treated C-doped sample (181 $\mu A/cm^2$), which is in turn 68% higher than that produced by the as-deposited C-doped TiO_2 (108 $\mu A/cm^2$). There is also a 29% increase in photocurrent density for MW plasma-treated C-doped coating compared to the MW plasma-treated un-doped sample (167 $\mu A/cm^2$). These increases in photocurrent density can be correlated with the band gap measurements in Fig. 5a and confirm that amorphous TiO_2 is less photoactive than its crystalline forms [8] while C-doping further increases the coating's photoactivity performance. The MW plasma treatment was also found to produce more photoactive coatings. There are a number of possible explanations for this, firstly the rougher

surface morphology and consequently the higher available surface area of the MW plasma-treated coating. A second factor is that the mixed-phase coating produced by MW plasma treatment has a higher content of anatase to rutile than that produced by furnace treatment at the same treatment temperature. A further factor could be related to the retention of more doped carbon in the MW plasma-treated sample; this could have further reduced the band gap of MW plasma-treated versus furnace-treated coating.

4. Conclusions

The use of MW plasma treatment was successfully demonstrated as a processing technique to convert amorphous TiO_2 and its C-doped coatings into their crystalline phases of anatase and/or rutile. The MW plasma-treated coatings were found to possess comparable crystallinity to the furnace-treated samples and yet this was achieved with an 83% reduction in overall processing time. Coatings treated by MW plasma also demonstrated higher photocurrent density possibly as a result of higher level of surface roughness and consequently a higher available surface area. Additionally, MW plasma-treated coatings also possess a higher content of anatase to rutile as well as a retention of more doped carbon, both of which further enhance the coatings' photoactivity.

C-doping was confirmed to effectively lower the band gap energy of the coatings and result in more photoactive coatings. Dopant content was also shown to influence the anatase-to-rutile phase transformation: the higher the carbon dopant content, the more favorable is the rutile formation. Treatment environment, whether oxygen-deficient or oxygen-abundant, demonstrated little effect on the anatase-to-rutile transition. These observations suggest that the phase composition (hence band gap energy and photoactivity) as well as the surface morphology of a

TiO_2 coating can be tailored to a specific application by alternating the level of C-doping and/or thermal treatment conditions.

Acknowledgments

The authors wish to acknowledge the grant of Science Foundation Ireland for funding this work through the Strategic Research Cluster on Solar Energy Conversion (Project No. 07/SRC/B1160).

References

[1] A. Fujishima, K. Honda, Nature, 238 (1972) 37-38.
[2] A. Fujishima, X.T. Zhang, D.A. Tryk, Surface Science Reports, 63 (2008) 515-582.
[3] O. Khaselev, J.A. Turner, Science, 280 (1998) 425-427.
[4] X. Chen, S.S. Mao, Chemical Reviews, 107 (2007) 2891-2959.
[5] S. Swann, Physics in Technology, 19 (1988) 67-75.
[6] L.J. Meng, M. Andritschky, M.P. Dossantos, Thin Solid Films, 223 (1993) 242-247.
[7] M.H. Suhail, G.M. Rao, S. Mohan, Journal of Applied Physics, 71 (1992) 1421-1427.
[8] M. Rahman, D. MacElroy, D.P. Dowling, Journal of Nanoscience and Nanotechnology, (2011) In press.
[9] P.I. Gouma, P.K. Dutta, M.J. Mills, Nanostructured Materials, 11 (1999) 1231-1237.
[10] C.H. Heo, S.B. Lee, J.H. Boo, Thin Solid Films, 475 (2005) 183-188.
[11] R.J.H. Clark, The Chemistry of Titanium and Vanadium, Elsevier, New York, 1968.
[12] L. Chen, M.E. Graham, G.H. Li, K.A. Gray, Thin Solid Films, 515 (2006) 1176-1181.
[13] Y.H. Tseng, C.S. Kuo, C.H. Huang, Y.Y. Li, P.W. Chou, C.L. Cheng, M.S. Wong, Nanotechnology, 17 (2006) 2490-2497.
[14] P.W. Chou, S. Treschev, P.H. Chung, C.L. Cheng, Y.H. Tseng, Y.J. Chen, M.S. Wong, Applied Physics Letters, 89 (2006).
[15] A. Testino, I.R. Bellobono, V. Buscaglia, C. Canevali, M. D'Arienzo, S. Polizzi, R. Scotti, F. Morazzoni, Journal of the American Chemical Society, 129 (2007) 3564-3575.
[16] P.W. Chou, Y.S. Wang, C.C. Lin, Y.J. Chen, C.L. Cheng, M.S. Wong, Surface & Coatings Technology, 204 (2009) 834-839.
[17] S.A. Borkar, S.R. Dharwadkar, Journal of Thermal Analysis and Calorimetry, 78 (2004) 761-767.
[18] S.U.M. Khan, M. Al-Shahry, W.B. Ingler, Science, 297 (2002) 2243-2245.
[19] M.L. McConnell, D.P. Dowling, C. Pope, K. Donnelly, A.G. Ryder, G.M. O'Connor, Diamond and Related Materials, 11 (2002) 1036-1040.
[20] H.L. Lu, G. Scarel, M. Alia, M. Fanciulli, S.J. Ding, D.W. Zhang, Applied Physics Letters, 92 (2008).
[21] R.A. Spurr, H. Myers, Analytical Chemistry, 29 (1957) 760-762.
[22] L. Vayssieres, On Solar Hydrogen & Nanotechnology, 1 ed., John Wiley & Sons, 2010.
[23] D. Mardare, M. Tasca, M. Delibas, G.I. Rusu, Applied Surface Science, 156 (2000) 200-206.
[24] S. Tanemura, L. Miao, W. Wunderlich, M. Tanemura, Y. Mori, S. Toh, K. Kaneko, Science and Technology of Advanced Materials, 6 (2005) 11-17.

Tables

Table 1. Comparison of un-doped and 2.2% C-doped TiO_2 coatings heat-treated by furnace and MW plasma.

	Un-doped		**2.2% C-doped**	
	MW plasma	**Furnace**	**MW plasma**	**Furnace**
a. Phase composition	100% Anatase	100% Anatase	66% Anatase 34% Rutile	62% Anatase 38% Rutile
Crystallite size*				
Anatase (101)	40 nm	44 nm	28 nm	28 nm
Rutile (110)	N/A	N/A	9 nm	10 nm
b. Surface roughness (Si wafer substrate)				
R_a	2.9 ± 0.2 nm	2.2 ± 0.2 nm	3.3 ± 0.5 nm	2.4 ± 0.2 nm
R_q	11 ± 4 nm	2.9 ± 0.4 nm	8 ± 2 nm	4 ± 1 nm

* Crystallite size is calculated using Scherrer Formula.

Figure captions

Fig. 1 (a) Oxygen, titanium, and carbon (total carbon and carbide carbon) uptakes of C-doped TiO_2 films as-deposited at 1 – 5 sccm of CO_2 and (b) XPS spectra of C1s state for the as-deposited, MW plasma-treated, and furnace-treated 2.2% C-doped coatings.

Fig. 2: Evolution of XRD patterns for the as-deposited (a) un-doped and (b) 2.2% C-doped TiO_2 upon MW plasma treatment. A relatively small reduction in coating thickness (from ~250 nm to ~200 nm) was also observed for samples heat-treated at higher temperatures, which may explain the enhancement in the intensity of Si(100) peak.

Fig. 3: Rutile mass fraction of MW plasma-treated C-doped TiO_2 films deposited at 1 – 5 sccm of CO_2.

Fig. 4: Surface morphology of 2.2% C-doped TiO_2 (a) furnace-treated and (b) MW plasma-treated at 750°C for 3 minutes.

Fig. 5: (a) Band gap and (b) photocurrent density measurements for as-deposited, MW plasma-treated, furnace-treated 2.2% C-doped and MW plasma-treated un-doped TiO_2 coatings. All heat treatments were performed at 750°C for 3 minutes.

Figures

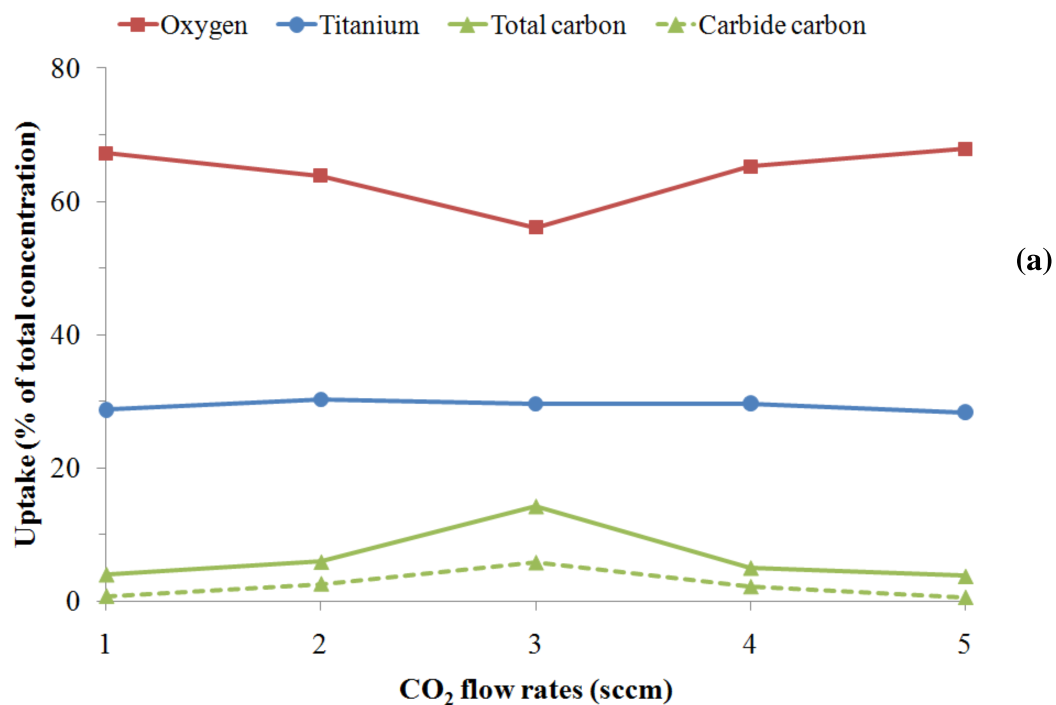

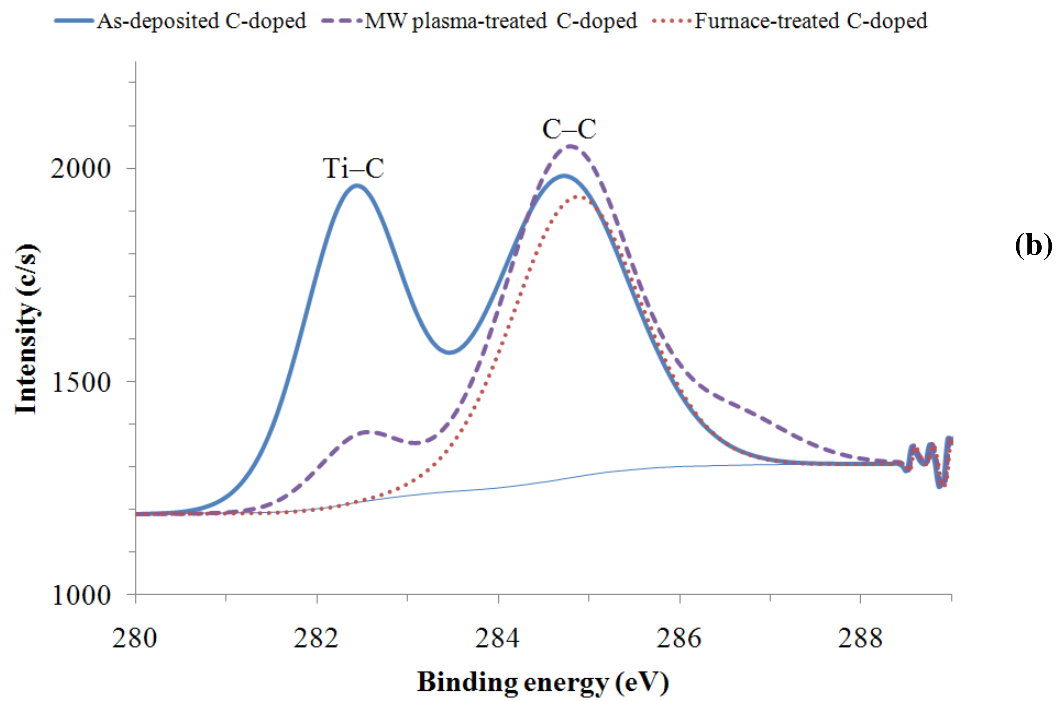

Fig. 1

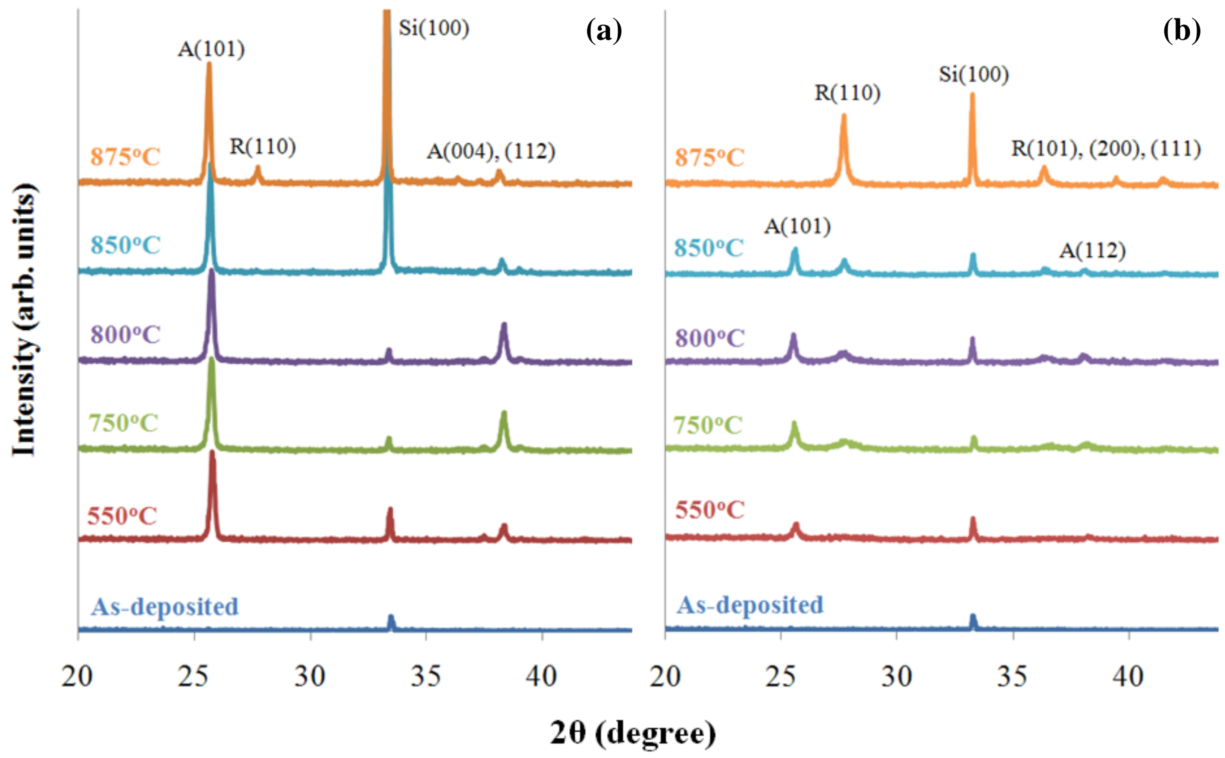

Fig. 2

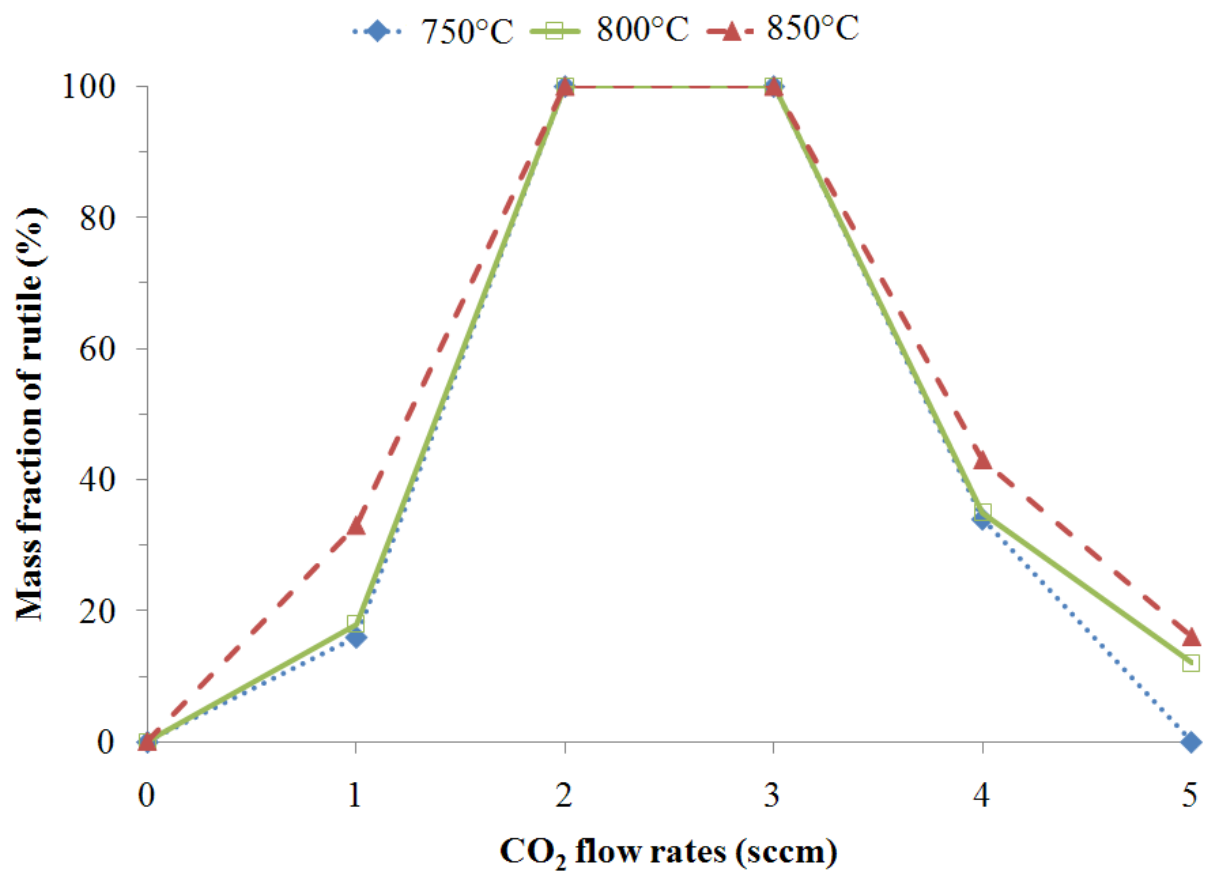

Fig. 3

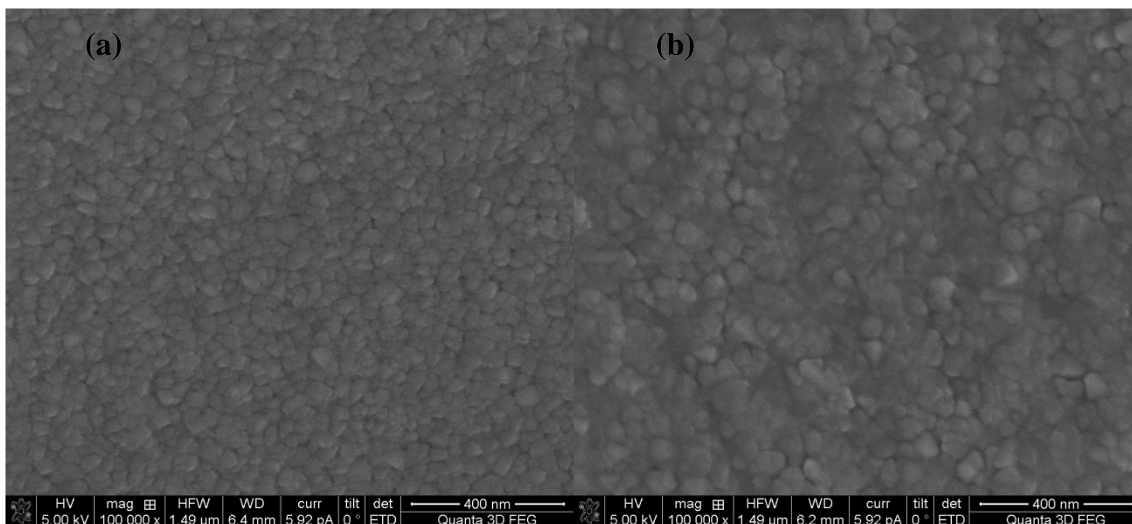

Fig. 4

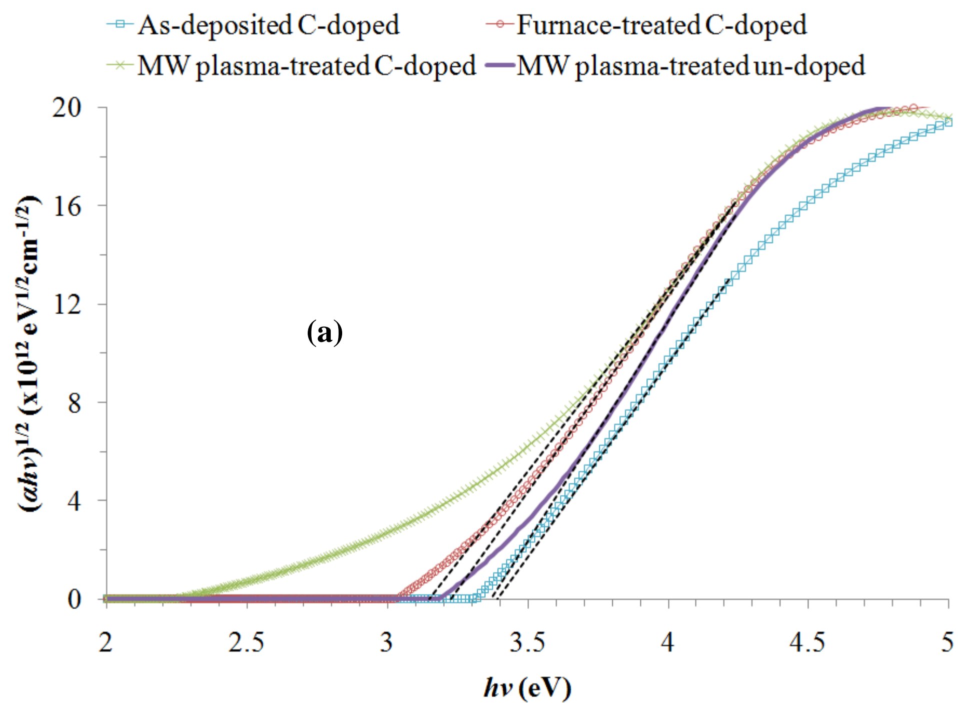

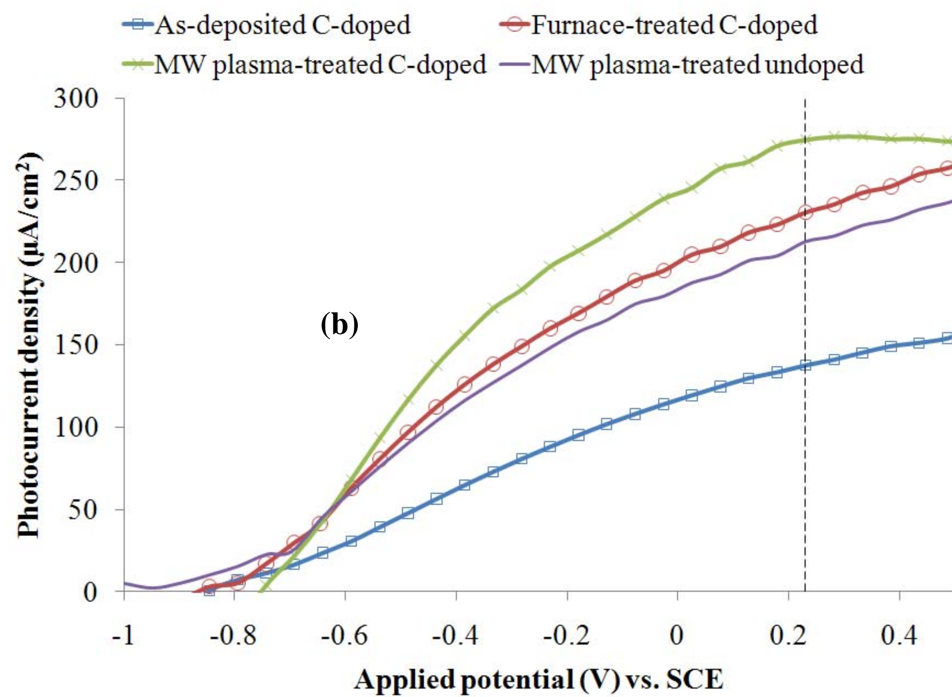

Fig. 5